ORCA – Online Research @ Cardiff

This is an Open Access document downloaded from ORCA, Cardiff University's institutional repository:https://orca.cardiff.ac.uk/id/eprint/129344/

This is the author's version of a work that was submitted to / accepted for publication.

Citation for final published version:

Robinson, Andrew J., Hopkins, Goitseone L., Rastogi, Namrata, Hodges, Marie, Doyle, Michelle, Davies, Sara, Hole, Paul S., Omidvar, Nader, Darley, Richard L. and Tonks, Alex 2020. Reactive oxygen species drive proliferation in acute myeloid leukemia via the glycolytic regulator PFKFB3. Cancer Research 80 (5) , pp. 937-949. 10.1158/0008-5472.CAN-19-1920

Publishers page: http://dx.doi.org/10.1158/0008-5472.CAN-19-1920

Please note:
Changes made as a result of publishing processes such as copy-editing, formatting and page numbers may not be reflected in this version. For the definitive version of this publication, please refer to the published source. You are advised to consult the publisher's version if you wish to cite this paper.

This version is being made available in accordance with publisher policies. See http://orca.cf.ac.uk/policies.html for usage policies. Copyright and moral rights for publications made available in ORCA are retained by the copyright holders.

Article Title: **Reactive oxygen species drive proliferation in acute myeloid leukemia via the glycolytic regulator PFKFB3**

Running Title: ROS drives proliferation in AML via PFKFB3

Article Type: Original Article

Key Words: Acute Myeloid Leukemia, Reactive Oxygen Species, Metabolism, Glycolysis, Proliferation.

Authors/Affiliations: Andrew J. Robinson,[1] Goitseone L. Hopkins,[1] Namrata Rastogi,[1] Marie Hodges,[1,2] Michelle Doyle,[1,2] Sara Davies,[1] Paul S. Hole,[1] Nader Omidvar,[1] Richard L. Darley[1] and Alex Tonks[1‡,¥]

[1]Department of Haematology, Division of Cancer & Genetics, School of Medicine, Cardiff University, Wales, United Kingdom.

[2]Cardiff Experimental and Cancer Medicine Centre (ECMC), School of Medicine, Cardiff University, Wales, United Kingdom.

[¥]**Funding**:

This work was supported by grants from Tenovus Cancer Care (A.R), Bloodwise (13029), Medical Research Council (G.L.H.), Health and Care Research Wales (G.L.H; H07-3-06), Cancer Research UK (C7838/A25173) and Sêr Cymru II Fellow supported by Welsh Government, European Regional Development Fund (NR; 80762-CU-182)

[‡]**Corresponding author:** Dr Alex Tonks, Department of Haematology, Division of Cancer & Genetics, School of Medicine, Cardiff University, Wales, UK.
Phone Number: ++44(0)2920742235
Email: Tonksa@cf.ac.uk
Twitter: @alex_tonks

Conflict of interest: The authors declare no conflict of interest.

Manuscript length:

Abstract: 189
Manuscript length: 5313
References: 52
Figures: 7 figures
Supplemental files: 12 Supplemental Figures and 2 Supplemental Tables

Abstract

Acute myeloid leukemia (AML) is a heterogeneous clonal disorder with a poor clinical outcome. Previously we showed that overproduction of reactive oxygen species (ROS), arising from constitutive activation of NOX2 oxidase, occurs in >60% of AML patients and that ROS production promotes proliferation of AML cells. We show here that the process most significantly affected by ROS overproduction is glycolysis. Whole metabolome analysis of 20 human primary AML showed that blasts generating high levels of ROS have increased glucose uptake and correspondingly increased glucose metabolism. In support of this, exogenous ROS increased glucose consumption whilst inhibition of NOX2 oxidase decreased glucose consumption. Mechanistically, ROS promoted uncoupling protein 2 (UCP2) protein expression and phosphorylation of AMPK, upregulating the expression of a key regulatory glycolytic enzyme, 6-phosphofructo-2-kinase/fructose-2,6-bisphosphatase (PFKFB3). Overexpression of PFKFB3 promoted glucose uptake and cell proliferation, whilst downregulation of PFKFB3 strongly suppressed leukemia growth both in vitro and in vivo in the NSG model. These experiments provide direct evidence that oxidase-derived ROS promotes the growth of leukemia cells via the glycolytic regulator PFKFB3. Targeting PFKFB3 may therefore present a new mode of therapy for this disease with a poor outcome.

Significance

Findings show that ROS generated by NOX2 in AML cells promotes glycolysis by activating PFKFB3, and suggest PFKFB3 as a novel therapeutic target in AML.

53 **Introduction**

54 Reactive oxygen species (ROS) are a heterogeneous group of molecules and free radicals
55 generated as a by-product of mitochondrial oxidative phosphorylation and deliberately generated
56 via nicotinamide adenine dinucleotide phosphate (NADPH) oxidase (NOX) family proteins (1).
57 In particular, NOX2 is expressed in the plasma membrane of hematopoietic cells that generates
58 superoxide. Superoxide rapidly dismutates to hydrogen peroxide (H_2O_2), a relatively long-lived,
59 mildly reactive molecule that traverses biological membranes and mediates redox signaling in
60 both autocrine and paracrine fashion (2). The capacity of H_2O_2 to reversibly oxidise cysteine
61 residues in regulatory domains or active sites of proteins is believed to underlie its biological
62 effects (3). Indeed, H_2O_2 plays an integral role in hematopoiesis both through direct and indirect
63 regulation of gene expression (4).

64 Excessive production of ROS is a common feature of cancer. In leukemia, ROS are known to
65 cause DNA damage (5) and also promote proliferation (6-8). We previously showed that >60%
66 of AML patients exhibited elevated levels of extracellular superoxide and H_2O_2 which correlated
67 with NOX2 expression (6). We also found that RAS (which is both directly and indirectly
68 activated in AML (9)) was able to drive the production of NOX2-derived ROS in normal
69 hematopoietic stem / progenitor cells (HSPC) and using this model we were able to show that
70 RAS-induced ROS production contributed to the pro-proliferative effects of this oncogene (7).
71 Despite this, the underlying mechanism through which ROS promote proliferation in cancer
72 remains unclear. Using this model, we show for the first time that ROS particularly impacts on
73 genes associated with the glycolytic pathway, with a key glycolytic regulator, PFKFB3, acting as
74 an important mediator of ROS. Correspondingly, we show that ROS also promotes glycolysis in

75 cell lines and AML patient blasts. Furthermore, myeloid leukemia cells exhibit dependency on
76 PFKFB3 both for their growth and survival. Given the frequently elevated levels of ROS in
77 primary AML, these data provide a plausible mechanism for the enhanced glycolysis seen in
78 AML and suggest that a therapeutic opportunity exists in which agents inhibiting PFKFB3 could
79 be used to treat this disease.

80 Materials and Methods

81 Key resources

82 All reagents and key resources are provided in Supplemental material.

83 Primary cell material and cell culture

84 For whole cell metabolomics, a subset of bone marrow samples (n=20) from AML patients who
85 had enrolled in UK MRC/NCRI AML clinical trials at point of diagnosis, before treatment and
86 obtained informed written consent from patients in accordance with the 1964 Declaration of
87 Helsinki, was used. Control mononuclear cells were isolated from peripheral blood of human
88 male/female volunteers (n=6).

89 Human neonatal cord blood was obtained from healthy full-term pregnancies at the University
90 Hospital Wales, Cardiff, UK. These were obtained with informed consent and with approval
91 from the South East Wales Research Ethics Committee in accordance with the 1964 Declaration
92 of Helsinki. Human $CD34^+$ cells (>95% pure, which constitute a mixed progenitor blood cell
93 population) were isolated, cultured and transduced with retroviral vectors based on the PINCO
94 backbone harboring either a GFP or DsRED selectable marker as previously described (10).
95 Transduced human $CD34^+$ hematopoietic progenitor cells were cultured in supplemented IMDM

96 as previously described (10) containing 20% *v/v* FCS; supplemented with 5 ng/mL human (hu)
97 IL-3, huG-CSF and huGM-CSF and 20 ng/mL huSCF. For microarray studies, on day 5 of
98 culture (post $CD34^+$ isolation), cells were washed in PBS and resuspended in supplemented
99 IMDM in the presence or absence of 100nM diphenyleneiodonium (DPI) for 18 h prior to
100 Affymetrix microarray (n=4). RNA was extracted using Trizol® as previously described (11).
101 Due to the high frequency of retroviral transduction (~70%), enrichment of transduced cells was
102 unnecessary.

103 Cell lines were purchased from ATCC or ECACC and cultured according to recommended
104 conditions at 37°C, 5% CO_2 for all experiments. All lines are maintained at ≤ 20 passage from
105 receipt. The genetic identity of the cell lines was confirmed by short tandem repeat (STR) at
106 purchase. Monthly monitoring for Mycoplasma contamination was performed and confirmed
107 using the MycoAlert Detection Kit (Sigma). Mice were bred and maintained at Cardiff
108 University (UK) and were cared for in accordance with Institutional Animal Care and Use
109 Committee guidelines. NOD-SCID IL2R$\gamma^{(-/-)}$(NSG) female mice were sub-lethally irradiated
110 with 200cGy total body irradiation 24h before inoculation of THP-1 cells via tail-vein injection.
111 Transplanted cells were analysed using hCD45-FITC, hCD33-APC and mCD45-PerCP-Cy5.5 by
112 flow cytometry. For *ex vivo* analysis of mouse MRP8 N-RAS^{G12D} leukemia (12), bone marrow
113 was harvested from the tibias and glucose uptake was measured using 2-NBDG as described
114 below.

115 **Detection of superoxide**

116 Following gene transduction, the indicated cell cultures were adjusted for viable cell number and
117 superoxide measurement was carried out using the chemiluminescent probe Diogenes™

118 (Geneflow, U.K.). Briefly, cells were resuspended in their conditioned medium to a density of
119 $1x10^6$ cells/mL and 150 µL aliquots were assayed in triplicate in FluoroNunc Maxisorp 96 well
120 plates (Thermo-Fisher Scientific, Loughborough, UK). Diogenes (50 µL) was added
121 immediately prior to recording chemiluminescence as previously described (7).
122
123 **Determination of glucose and lactate**
124 Supernatant from the culture media was filtered using Microcon-10 kDa centrifugal filter units
125 (Merck-Millipore, Feltham, UK) at 12,782 × g for 30 min. The levels of D-glucose and L-
126 Lactate were measured by fluorimetry using a glucose and L-Lactate assay kit (Abcam,
127 Cambridge, UK) coupled with a Chameleon Hidex fluorescent plate reader (Ex/Em 535/590 nm),
128 according to the manufacturer's instructions. Briefly, samples were diluted with proprietary
129 glucose or lactate buffer to a volume of 50µL and added in triplicate to a black 96 well flat
130 bottomed microclear plate (Greiner Bio-One, Stonehouse, UK). Glucose or lactate buffer
131 containing proprietary glucose or lactate probe (0.8% *v/v*) and proprietary glucose or lactate
132 enzyme mix (0.8% *v/v*) were added (50µL) to each well and left to incubate in the dark at RT for
133 30 min. Fluorescence was measured (Ex/Em 535/590nm) and compared with glucose or lactate
134 standards assayed in duplicate on the same plate.

135 To determine cellular glucose uptake at the individual cell level, the glucose bioprobe 2-NBDG
136 (Life Technologies, U.K.) was employed in conjunction with flow cytometry. Cells were
137 washed twice in PBS then treated with 2-NBDG (10µM) or PBS alone (to establish a
138 background control) followed by incubation for 10 min (37^oC, 5% CO_2) and two washes in ice
139 cold PBS. Cells were immediately analysed by flow cytometry using an Acurri C6 flow
140 cytometer. 2-NBDG emits fluorescence at a wavelength of 542nM. Having excluded cell debris

141 based on FSC/SSC, the median glucose uptake per cell of the samples was established by
142 subtracting the median value of fluorescence of the background control cells from the median
143 value of fluorescence of the cells treated with 2-NBDG. In some experiments, cells were treated
144 with PEGylated catalase (300 mU/mL) for 24 h at 37°C, prior to analysis of glucose uptake.

145 **Expression analysis**

146 Transduced CD34^{+} cells were washed in PBS and resuspended in supplemented IMDM in the
147 presence or absence of 100nM diphenyleneiodonium (DPI) for 18 h prior to RNA isolation (n=4)
148 as previously described (11). RNA was hybridized to Affymetrix GeneChip® Human Exon 1.0ST
149 Array for whole-transcript expression analysis. Data were analysed using Partek Genomics Suite
150 (v6.6; Partek, MO, USA). Data analysis of CEL files are described in Supplemental Methods;
151 data available at https://www.ebi.ac.uk/arrayexpress (accession number e-mexp-583). Gene
152 Ontology (GO) enrichment analysis was undertaken using Metacore® (Clarivate Analytics,
153 U.K.).

154 Detection of each protein was determined by western blot using antibodies described in
155 Supplemental Methods, in conjunction Amersham ECL™ Advance/Prime Western Blotting
156 Detection Kit (GE Healthcare U.K.).

157 **Metabolomics**

158 Metabolomic analysis of AML patient blast samples or Mv4;11 was carried out by Metabolon™
159 (http://www.metabolon.com/). Data was generated using ultra-high performance liquid
160 chromatography-tandem mass spectroscopy (UPLC-MS/MS) and gas-chromatography mass-
161 spectroscopy (GC-MS). Peripheral blood and bone marrow samples collected from a random

162 cohort of AML patients were counted and analysed for viability using 7-AAD. Only those
163 samples with a cell count greater than 30 million and a viability greater than 80% were sent for
164 analysis by Metabolon™ (n=20). Additionally, mononuclear cells isolated from healthy
165 individuals (n=6) were also sent to Metabolon™ as a comparative control. Diogenes™ analysis
166 of AML blasts stratified the patient samples into ROS^{High} (above median) and ROS^{Low} (below
167 median). Raw data was extracted, peak identified and quality control processed using
168 proprietary Metabolon™ hardware, software and biochemical library database. Following
169 normalisation to Bradford protein concentration, log transformation and imputation of missing
170 values with the minimum observed value for each compound, Welch's unequal variance two
171 sample t-test was performed to identify significant differences between the experimental groups.
172 To account for a potentially high false discovery rate (as a consequence of multiple
173 comparisons), a q-value was also calculated, where a lower q-value is an indication of higher
174 confidence in the result.

175 **Protein expression analysis of genes identified by microarray analysis**

176 Detection of each protein (see key resources table) was determined using a monoclonal or
177 polyclonal antibody in conjunction with an anti-mouse or anti-Rabbit HRP linked secondary
178 antibody and Amersham ECL™ Advance/Prime Western Blotting Detection Kit (GE Healthcare
179 UK) according to the manufacturer's instruction. In the case of NOX2 or glucose transporter cell
180 surface protein expression, PE conjugated antibody to NOX2 epitope or an indirect stain coupled
181 with anti-mouse IgG-APC was used and protein expression was determined by flow cytometry.

182 **Flow cytometric and data analysis**

183 Flow cytometric data were acquired using an Accuri C6 cytometer (BD, U.K.). Data analysis
184 was performed using FCS express v6 (DeNovo Software). The threshold for GFP positivity was
185 determined from the autofluorescence of GFP/DsRED negative cells in mock transduced
186 cultures. Significance of difference was tested using Minitab software version 19 (Minitab Inc,
187 PA) all analyses except those provided by Metabolon assays (see above). Appropriate statistical
188 tests used are labelled in figure legends. To better understand variations between samples,
189 principal component analysis (PCA) or hierarchical clustering using distance Pearson Correlation
190 was employed to provide a global analysis of how closely related or otherwise any given sample
191 is (mRNA or biochemical).

192 ## Results

193 **NOX-derived ROS promotes transcriptional change in N-RAS^{G12D} expressing**
194 **hematopoietic progenitor cells and AML patient blasts**

195 We previously showed that expression of N-RAS^{G12D} in HSPC strongly promotes ROS
196 production through activation of NOX oxidases leading to increased proliferation (7). We used
197 this model of ROS overproduction in primary hematopoietic CD34^{+} cells (Supplemental Fig.
198 S1A-E) to investigate the changes in gene expression mediated by ROS. We reasoned that we
199 could enrich for ROS target genes by looking for gene changes which were absent in mutant N-
200 RAS^{G12D} cells treated with the NOX inhibitor, DPI (Fig. 1A). N-RAS^{G12D} significantly changed
201 the expression of 305 genes in HSPC ($p<0.05$) (Supplemental Table S1) of which 24 were
202 specifically attributed to ROS production. Metacore^{TM} pathway analysis identified glycolysis as
203 the most dysregulated pathway (Fig. 1B). ROS significantly impacted the expression of 18% of
204 genes involved in carbohydrate metabolism (Fig. 1C). To examine this in AML patient blasts,

205 we analyzed the TCGA database of 161 AML patients using cBioPortal (13, 14). Hierarchical
206 clustering in Fig. 1D shows that patients with high NOX2 (*CYBB*) expression (which we have
207 previously shown to correlate with ROS production (7)) clustered together based on correlative
208 expression of genes involved in carbohydrate metabolism suggesting changes in glucose
209 utilization compared to those patients with lower NOX2 expression; more than half the ROS
210 regulated genes observed above are seen in this cluster. Fig. 1E shows the ROS-responsive
211 genes that significantly correlated with NOX2 expression in AML blasts. Data derived from
212 TCGA (15) supports the overexpression of *NOX2* mRNA in AML (Supplemental Fig. S2A).
213 Increased *NOX2* expression also showed a trend towards poor prognosis (P=0.075; Supplemental
214 Fig. S2B). We did not observe any significant association of expression of genes identified in
215 Fig.1E with AML cytogenetics or survival. Taken together, these data show that NOX inhibition
216 upregulates the expression of genes involved in carbohydrate metabolism.

217 **ROS promotes functional changes in glucose uptake**

218 Increased aerobic glycolysis is a common feature of cancerous cells with concomitant increases
219 in cellular glucose uptake and lactate secretion (16). In order to assess whether transcriptional
220 changes observed above resulted in functional glycolytic changes, glucose uptake and lactate
221 secretion were measured. The level of glucose taken up by N-RAS^{G12D} HSPC was significantly
222 more (48±19%) when compared to control (Fig. 2A) when analysing glucose remaining in the
223 culture media. To confirm that these changes in cellular glucose consumption occurred at the
224 single cell level, the fluorescent glucose bioprobe 2-NBDG was employed (Supplemental Fig.
225 S3). N-RAS^{G12D} increased glucose uptake by 36±15% compared to controls (Fig. 2A). To
226 support these *in vitro* data, glucose uptake was assayed *ex vivo* in bone marrow cells harvested
227 from secondary transplants of transgenic mice expressing N-RAS^{G12D} (12). A significant

228 90±48% increase in glucose uptake was observed in N-RAS^{G12D} mice compared to wild type
229 control (Fig. 2B). These data demonstrate that expression of mutant N-RAS^{G12D} increases
230 glucose uptake both *in vitro* and *ex vivo*.

231 To assess whether increases in glucose uptake were mediated by NOX-derived ROS, we
232 examined the effect of the NOX inhibitor, DPI, on N-RAS^{G12D} HSPC. NOX inhibition reduced
233 glucose uptake by 20% compared to untreated cells (Fig. 2C) when analysing glucose remaining
234 in the culture media. Similar data were obtained with the alternative NOX inhibitor, VAS-2870
235 (17). Treatment with PEGylated catalase (which catabolises the destruction of H_2O_2 at the
236 plasma membrane (18)) also reverted the increase in glucose uptake (Fig. 2C). In contrast,
237 treatment of control HSPC with DPI or VAS-2870 had no significant effect on glucose uptake.
238 To determine whether these changes in glucose uptake resulted in increases in extracellular
239 lactate production, levels of L-lactate in the culture supernatant were assayed. Interestingly, no
240 significant changes in lactate secretion (see below) was observed in cells expressing N-RAS^{G12D}
241 compared to control (Fig. 2D).

242 **Overproduction of ROS is associated with changes in glucose utilization in primary AML**
243 **blasts**

244 The above data suggests increased glucose uptake is at least in part mediated by production of
245 NOX-derived ROS. To establish evidence for this in primary AML, we stratified AML blasts
246 according to extracellular ROS production (ROS^{High} and ROS^{Low}; Supplemental Fig. S4A-B) and
247 analysed the global biochemical metabolomic profile. Using this approach, 444 named
248 metabolites were identified which distinguished ROS^{High}, ROS^{Low} and control MNC by PCA
249 (Fig. 3A). A summary of the biochemicals that achieved statistical significance ($p \leq 0.05$) or

250 approached it ($0.05<p<0.10$), is shown in Fig. 3B and in full in Supplemental Table S2. Random
251 Forest (RF) analysis of the cellular metabolic profiles resulted in 85% predication accuracy in
252 differentiating ROS^{High} and ROS^{Low} groups (Supplemental Fig. S5). Among the 30 top-ranking
253 metabolites resulting from the RF analyses were biochemicals spanning different pathways, but
254 primarily limited to those associated with nucleotides and lipid metabolism. Polyunsaturated
255 fatty acids and lipid-related changes in n3 and n6 polyunsaturated fatty acids showed significant
256 accumulations within the AML^{High} compared to the AML^{Low} samples which would be indicative
257 of increased uptake (Supplemental Table S2). Interesting, within the AML^{High} samples,
258 lysolipids, monoacylglycerols and glycerol were consistently and significantly higher in relation
259 to AML^{Low} ROS (see discussion).

260 Focussing specifically on detected metabolites within the glycolytic pathway, we found, glucose,
261 glucose-6-phosphate and fructose-6-phosphate levels were significantly higher within the
262 ROS^{High} blasts compared to ROS^{Low} blasts indicating that increased glucose utilisation correlates
263 with elevated ROS (Fig. 3C). In agreement with our *in vitro* HSPC model, changes in lactate
264 were not significantly different between the ROS high and ROS low groups but were higher than
265 the control MNC (Fig. 3C). This suggests that whilst glucose utilisation is increased in primary
266 AML, higher levels of ROS are consistent with increased levels of glycolytic intermediates.
267 Indeed, metabolites associated with the pentose phosphate pathway (PPP) including the isobaric
268 compound ribulose/xylulose 5-phosphate and sedoheptulose-7-phosphate were also higher in
269 ROS^{High} *vs* ROS^{Low} samples (Fig. 3D). We next set out to determine whether the addition of
270 exogenous H_2O_2 to the ROS^{Low} AML cell line, Mv4;11 could itself promote changes in glucose
271 metabolism. Similarly to primary AML-ROS^{high} we observed an increase in glucose
272 consumption (Fig. 4) and biochemicals associated with the PPP (Supplemental Fig. S6A and B).

273 Taken together these data suggests increased glucose utilization by PPP, potentially driving
274 nucleotide biosynthesis and NAD(P)H generation within ROS^{High} blasts.

275 **PFKFB3 is a ROS responsive target that mediates changes in glucose utilization**

276 The data above suggest that ROS-induced changes in mRNA expression of genes of glycolysis
277 (Fig. 1C) was associated with altered glucose utilization (Fig. 3). To validate these findings, we
278 surveyed the expression of these ROS-responsive genes at the protein level (Supplemental Fig.
279 S7A-D). ROS induced changes at the protein level, only occurred in the expression of the
280 regulatory glycolytic enzyme 6-phosphofructo-2-kinase/fructose-2,6-bisphosphatase 3
281 (PFKFB3)(Fig. 4A and Supplemental Fig. S7A). PFKFB is a bifunctional enzyme with both
282 kinase and phosphatase activity that regulates the glycolytic pathway (19). To support this data,
283 we inhibited NOX derived ROS production in the ROS^{High} AML cell line, THP-1, using NOX2
284 knock-down (Supplemental Fig. S8A-C). In line with our previous data (7), NOX inhibition
285 with DPI suppressed proliferation of N-RAS^{G12D} cells. As shown in Fig. 4B, loss of NOX2
286 protein expression and ablation of superoxide production in these cells reduced the expression of
287 PFKFB3 compared to control cells with a concomitant reduction in proliferation by 30±12%
288 when compared to control (Fig. 4C). Glucose uptake was similarly reduced by 25±17% (Fig.
289 4D). We next set out to determine whether the addition of exogenous H_2O_2 to the ROS^{Low} AML
290 cell line, Mv4;11 cells, could itself promote PFKFB3 protein expression. As predicted, we
291 observed a dose-dependent increase in PFKFB3 protein expression (Fig. 4E) with concomitant
292 increases in proliferation (Fig. 4F and Supplemental Fig. S9) and glucose uptake (Fig. 4G).

293 To investigate whether PFKFB3 itself could mediate these phenotypic changes, we
294 overexpressed PFKFB3 in Mv4;11 cells (PFKFB3-OE; Fig. 5A). Cells overexpressing PFKFB3

295 showed a 72±30% increase in proliferation (at 72 h) compared to control cells (Fig. 5B) and
296 correspondingly showed an increased proportion of cells in S+G2M phase of the cell cycle
297 (Supplemental Fig. S10A). The levels of glucose uptake in PFKFB3-OE cells were significantly
298 more (35±2%) compared to control cells (Fig. 5C). To determine the impact of decreased
299 expression of PFKFB3 in ROS generating cells, PFKFB3 was knocked-down in THP-1 cells
300 (Fig. 5D). Knock-down of PFKFB3 resulted in reduced proliferation of these cells (Fig. 5E) and
301 a reduction in the percentage of cells in cycle (Supplemental Fig S10B), though without
302 detectable change in glucose uptake in this context (Fig. 5F). These experiments provide the
303 first direct evidence that PFKFB3 controls the growth of leukemia cells which is consistent with
304 cells producing high levels of ROS.

305 **ROS induced changes in PFKFB3 expression are mediated via UCP/p-AMPK**

306 To determine the mechanism of ROS induced PFKFB3 expression we analysed two potential
307 mechanisms. Firstly, HIF-1α has been shown to induce increased *PFKFB3* mRNA expression
308 (20). Analysing our transcriptome data revealed that *HIF-1α* is a strongly ROS-responsive gene
309 (Fig. 6A). However, we were unable to detect expression of HIF1-α protein regardless of NOX2
310 status (Fig. 6B). Furthermore, HIF1α knock-down (Fig. 6B) did not change PFKFB3 protein
311 expression (Fig. 6C) or glucose uptake (Fig. 6D). Collectively, these data do not therefore
312 support a role of HIF1-α in mediating glycolytic changes in these cells.

313 Superoxide levels are sensed by uncoupling protein 2 (UCP2) which drives an adaptive response
314 to protect against oxidative stress including the activation of AMP-activated protein kinase
315 (AMPK) (21) leading to increased production of PFKFB3 (22). In accord with this we observed

316 that treatment of the ROS^{Low} AML cell line, Mv4;11, with exogenous H_2O_2 increased both
317 PFKFB3 expression and AMPK phosphorylation (Fig. 6E). This induction was inhibited by
318 Genipin (which specifically inhibits UCP2 expression (23)) decreasing both p-AMPK and
319 PFKFB3 levels (Fig. 6D) and concomitant reduction in glucose consumption (Fig. 6F). To
320 confirm, changes in p-AMPK/mTOR signalling, we next examined downstream signalling of
321 mTOR by western blot. As shown in Supplemental Fig. S11A and B phosphorylation of S6
322 kinase is decreased following treatment with H_2O_2; an effect reversed when UCP2 is inhibited.
323 These data support a role for UCP2 having a pivotal role in mediating ROS-induced changes in
324 the expression of PFKFB3.

325 **Targeting PFKFB3 reduces glucose uptake and cell proliferation in AML cells**

326 We next wanted to establish whether chemical inhibition of PFKFB3 could have the potential for
327 a therapeutic impact in the treatment of AML. Having established appropriate inhibitory
328 concentrations of two chemical inhibitors of PFKFB3, 3-(3-pyridinyl)-1-(4-pyridinyl)-2-propen-
329 1-one (3PO) (24) and the more specific PFK158 (25) (Supplemental Fig. S12A-C). We next
330 treated ROS^{High} cells (THP-1) with 3-PO or PFK158 which resulted in a reduction in glucose
331 uptake (Fig. 7A and B). Correspondingly, treatment with 3PO resulted in a significant dose
332 dependent decrease in proliferation of THP-1 cells (Fig. 7C) whilst treatment with the more
333 specific PFK158 (25) also significantly reduced proliferation at doses >500nM (Fig. 7D). We
334 next investigated whether PFKFB3 inhibition could suppress the effects of exogenous ROS on
335 the ROS^{Low} cell line Mv4;11. No change in viability in Mv4;11 (or THP-1) cells treated with
336 3PO, PFK158 or H_2O_2 were observed. Treatment of Mv4;11 cells with H_2O_2 resulted in a
337 20±9% increase in glucose uptake compared with control (as expected), whilst combined
338 treatment with H_2O_2 and 3PO or with PFK158 inhibitor ablated the response to peroxide (Fig.

339 7E). Treatment with these inhibitors alone did not alter glucose uptake when compared to
340 control cells.

341 Finally, we investigated whether loss of PFKFB3 also affected leukemia growth *in vivo*. Knock-
342 down of PFKFB3 expression in THP-1 cells resulted in a significant reduction (83%) of
343 leukemia cell growth, supporting a role of PFKFB3 in the proliferation of AML cells *in vivo*
344 (Fig. 7F). Overall these experiments provide the first direct evidence that oxidase-derived ROS
345 promotes the growth of leukemia cells via PFKFB3 expression and suggests a potential ROS-
346 dependent mechanism for these changes.

347 Discussion

348 Whilst increased levels of ROS produced by AML blasts or tumor cells have been shown to
349 induce double strand breaks (26), they also promote proliferation (6, 27). Here we present
350 evidence that the proliferative response to ROS is supported by changes in glucose uptake and
351 altered glucose metabolism. Furthermore, we demonstrate that AML cells exhibit enhanced
352 PFKFB3 expression and that inhibitors that target the function of this protein (or its upstream
353 pathway UCP2/AMPK) may provide a tractable therapeutic target in AML.

354 ROS are now recognized as important secondary messengers, serving as critical cell signaling
355 molecules through the capacity of H_2O_2 to reversibly oxidise cysteine residues (28). Using a
356 primary cell model for ROS production, we investigated the effect of ROS on gene transcription
357 and found that changes in mRNA expression were associated with enzymes involved in glucose
358 metabolism. Specifically, we identified several gene changes associated with glycolysis coupled
359 with increased cellular glucose uptake. This is consistent with many solid tumor models that

360 shift energy production from oxidative phosphorylation toward the less efficient glycolytic
361 pathway, a phenomenon known as the Warburg effect (29). Indeed, our previous data have
362 shown no significant differences in mitochondrial ROS were observed in mutant Ras expressing
363 $CD34^+$ cells compared to controls (7). Using inhibitors to NOX2, we were able to attribute the
364 effects of observed increases in glucose uptake to the production of extracellular NOX2-derived
365 ROS. Additionally, we found leukemic cell lines increased glucose uptake in response to
366 exogenous ROS or showed decreased uptake following NOX2 knock-down. We show for the
367 first time that the effect of ROS on glucose uptake is mediated by PFKFB3 (see below).
368 However, pro-glycolytic effects of ROS on other genes have been observed (30) and is
369 consistent with increased glycolysis in solid tumor models associated with GLUT upregulation
370 (31).

371 In the context of primary AML, we previously demonstrated that >60% of patients exhibited
372 high levels of ROS which correlated with NOX2 expression (6). Here, AML blasts stratified
373 according to level of extracellular ROS production were analysed by global biochemical
374 metabolomic profiling. Several hundred metabolites were identified which distinguished
375 patients according to ROS production including metabolite levels within the glycolytic pathway
376 (glucose, glucose-6-phosphate and fructose-6-phosphate) suggesting that the impact of ROS is to
377 increase the levels of glycolytic intermediates, primarily those in the early part of the glycolytic
378 pathway. In support of this, metabolites associated with the PPP such as sedoheptulose-7-
379 phosphate and the isobaric compounds ribulose/xylulose 5-phosphate were also elevated in
380 ROS^{High} samples. These data may be indicative of a reprogramming of metabolic pathways,
381 where increased glucose consumption, is metabolised via the PPP, resulting in increased
382 generation of NADPH (to counter oxidative stress) and biosynthetic precursors such as

383 nucleotides, necessary for cell growth and DNA repair. Interestingly, metabolomic profiling of
384 serum from AML patients has also revealed distinct increases in the glycolytic metabolic (32,
385 33). Additionally, NOX2 expression has previously been demonstrated to regulate self-renewal
386 of leukemic stem cells (34). Using a murine model of leukemia, Adane *et al* showed that
387 suppression of NOX2 expression led to increased fatty acid oxidation and potential limiting of
388 substrates passing through glycolysis. Our study supports this notion, where we also observed
389 significant changes associated with lipid metabolism in human AML; lipid-related changes in n3
390 and n6 polyunsaturated fatty acids showed significant accumulations within the AML^{High} in
391 relation to the AML^{Low} samples. The higher levels of monoacylglycerols and glycerol in the
392 AML^{High} samples may also be an indicator of increased lipolysis to support free fatty acid levels.
393 Taken together, these data show that NOX2 derived ROS impact on glucose metabolism, an
394 effect consistent with that seen in solid tumors (35).

395 We identified significant ROS induced changes in mRNA and in protein of the regulatory
396 glycolytic enzyme PFKFB3. *PFKFB3* mRNA expression has been shown to be upregulated in
397 several solid tumors including colon, breast, prostate, ovary, thyroid and head and neck
398 squamous cell carcinoma (36, 37). Whilst *PFKFB3* mRNA is elevated in AML we did not
399 observe any significant association of expression with particular AML subgroups or clinical
400 outcome. PFKFB is a bifunctional enzyme, which catalyses both forward and reverse reaction of
401 F-6-P to F-2,6-BP (19). In turn, F-2,6-BP is a powerful allosteric activator of PFK which
402 catalyses F-6-P to F-1,6-BP, a rate limiting step in glycolysis. The PFKFB3 isoform contains a
403 lysine and serine at position 79 and 80 respectively (38) resulting in increased kinase activity,
404 which is 740 times greater than other PFKFB isoforms, making it a powerful driver of glycolysis
405 (39). Here we also showed ROS dependent changes in PFKFB3 expression in AML lines with

406 constitutive NOX2 activity/ROS production coupled with suppression of reduction in
407 proliferation and glucose uptake upon ROS inhibition. Overexpression/knock-down of PFKFB3
408 generated the predicted changes in glucose uptake and cell proliferation *in vitro* whilst knock-
409 down of PFKFB3 strongly suppresses leukemia growth *in vivo* (though we have not confirmed
410 what the mechanistic basis of the effects are, *in vivo* data).

411 It has previously been established that ROS can regulate HIF-1α in a non-hypoxic pathway (40).
412 Further, stabilisation of HIF-1α has been associated with increased expression of glycolytic
413 genes, including PFKFB3 (41, 42). Our data showed increased expression of *HIF-1α* mRNA
414 correlated with increased ROS levels. However, immunoblotting showed that HIF-1α was not
415 expressed at detectable levels and furthermore knock-down of the mRNA for this protein did not
416 result in any changes in glucose uptake. ROS has also previously been shown to activate
417 mitochondrial proteins (UCP2) to regulate the leak of protons across the inner membrane,
418 resulting in poor fuel conversion efficiency and a more pro-glycolytic phenotype including
419 AMPK activation (21). We show that inhibition of UCP2 led to decreased p-AMPK and
420 PFKFB3 levels. Further, analysis of the mTOR pathway showed decreased S6-Kinase
421 expression in response to ROS which was reverted upon UCP inhibition. AMPK is a master
422 regulator of cellular energy homeostasis, upregulating catabolic metabolic processes including
423 increased glycolytic flux and protects against ROS accumulation by increasing NADPH
424 production (see below) (17). AMPK has previously been shown to be activated via ROS (43), in
425 addition to regulating glycolysis and PFKFB3 expression in a phosphorylation dependent
426 manner in cancer cells (22, 44). Domenech *et al*., have shown that mitotic arrest of cancer cells
427 leads to altered energy requirements through switching to a more glycolytic phenotype and
428 increased AMPK phosphorylation (22). This suggests that PFKFB3 could also be increased

429 through changes to cell cycle or autophagy. Metabolomic data generated as part of this study
430 also indicated increased levels of ROS correlated with an increase in fatty acid metabolites
431 (Supplemental Table S2). Interestingly, changes in expression of UCP2 has been linked with 2-3
432 fold elevation of plasma fatty acids reviewed in (45). Further, activation of fatty acid
433 metabolism by AMPK (46) is interesting given that ROS activation of AMPK has also been
434 shown to potentially influence and maintain HSC (47). Conversely, inhibition of mitochondrial
435 fatty acid oxidation induces loss of HSC maintenance (48).

436 Identification of metabolic differences between normal and malignant tissue creates a therapeutic
437 opportunity for targeting of glycolysis in the treatment of AML; the potential for targeted therapy
438 in AML, through reduction of aberrant metabolic activity via inhibition of 6-phosphogluconate
439 dehydrogenase (6-PGD) function has also recently been shown (32). The therapeutic potential of
440 PFKFB3 inhibition (e.g. PFK158) (25) in cancer is currently undergoing phase I clinical trials
441 (49). Consistent with studies in solid tumors (50, 51), data presented here shows that in ROS^{High}
442 AML cells, treatment with PFKFB3 inhibitor significantly reduced glucose uptake and also
443 proliferation both *in vitro* and *in vivo*. This supports a previous study which showed chemical
444 inhibition of PFKFB3 in Jurkat T-cell leukemia cells results in decreased proliferation and
445 glucose uptake (24). In myeloproliferative neoplasms expressing JAK2 mutations, PFKFB3 is
446 required for increased growth and metabolic activity, an effect blocked by targeted knock-down
447 of PFKFB3. This study therefore suggested that therapies specifically blocking PFKFB3
448 activity/expression would be expected to inhibit JAK2/STAT5-dependent malignancies (52).

449 In conclusion, this and previous data suggest that production of ROS may confer a competitive
450 advantage on premalignant/malignant cells by promoting the proliferation of these cells via

451 changes to carbohydrate metabolism. We show for the first time a link between increased NOX-
452 derived ROS production and increased expression of the key glycolytic regulatory enzyme,
453 PFKFB3. Furthermore, PFKFB3 inhibitors or genetic knock-down established a causal link
454 between ROS production, cellular glucose uptake and PFKFB3 activity.

455 Acknowledgments

456 We are grateful to Nick Jones (Swansea University, Wales, UK) for critically appraising the
457 manuscript. We would also like to thank Megan Musson CBS, Cardiff University for her
458 technical expertise for Affymetrix Microarray. We are grateful to Prof Tee (Cardiff University)
459 for his expertise in AMPK/mTOR signalling advice. The authors are grateful for support from
460 the NCRI AML trials cell bank and the AML patients for providing primary samples used in this
461 study. This work was supported by grants from Tenovus Cancer Care (A.R), Bloodwise
462 (13029), Medical Research Council (G.L.H.) and Health and Care Research Wales (G.L.H; H07-
463 3-06). NR is a Sêr Cymru II Fellow supported by Welsh Government, European Regional
464 Development Fund (NR; 80762-CU-182).

465 Supplemental Information

466 Supplemental information is available at Cancer Research website.

467 References

468
469
470 (1) Lambeth JD, Neish AS. Nox enzymes and new thinking on reactive oxygen: a double-
471 edged sword revisited. Annu Rev Pathol 2014;**9**:119-45.

472 (2) Hole PS, Darley RL, Tonks A. Do reactive oxygen species play a role in myeloid
473 leukemias? Blood 2011;**117**:5816-26.

474 (3) Bindoli A, Rigobello MP. Principles in redox signaling: from chemistry to functional
475 significance. Antioxid Redox Signal 2013;**18**:1557-93.

476 (4) Prieto-Bermejo R, Romo-Gonzalez M, Perez-Fernandez A, Ijurko C, Hernandez-
477 Hernandez A. Reactive oxygen species in haematopoiesis: leukaemic cells take a walk on
478 the wild side. J Exp Clin Cancer Res 2018;**37**:125.

479 (5) Mesbahi Y, Zekri A, Ghaffari SH, Tabatabaie PS, Ahmadian S, Ghavamzadeh A.
480 Blockade of JAK2/STAT3 intensifies the anti-tumor activity of arsenic trioxide in acute
481 myeloid leukemia cells: Novel synergistic mechanism via the mediation of reactive
482 oxygen species. Eur J Pharmacol 2018;**834**:65-76.

483 (6) Hole PS, Zabkiewicz J, Munje C, Newton Z, Pearn L, White P, et al. Overproduction of
484 NOX-derived ROS in AML promotes proliferation and is associated with defective
485 oxidative stress signaling. Blood 2013;**122**:3322-30.

486 (7) Hole PS, Pearn L, Tonks AJ, James PE, Burnett AK, Darley RL, et al. Ras-induced
487 reactive oxygen species promote growth factor-independent proliferation in human
488 CD34+ hematopoietic progenitor cells. Blood 2010;**115**:1238-46.

489 (8) Jayavelu AK, Moloney JN, Bohmer FD, Cotter TG. NOX-driven ROS formation in cell
490 transformation of FLT3-ITD-positive AML. Exp Hematol 2016;**44**:1113-22.

491 (9) Qian X, Nie X, Yao W, Klinghammer K, Sudhoff H, Kaufmann AM, et al. Reactive
492 oxygen species in cancer stem cells of head and neck squamous cancer. Semin Cancer
493 Biol 2018;**53**:248-57.

494 (10) Tonks A, Pearn L, Tonks AJ, Pearce L, Hoy T, Phillips S, et al. The AML1-ETO fusion
495 gene promotes extensive self-renewal of human primary erythroid cells. Blood
496 2003;**101**:624-32.

497 (11) Tonks A, Pearn L, Musson M, Gilkes A, Mills KI, Burnett AK, et al. Transcriptional
498 dysregulation mediated by RUNX1-RUNX1T1 in normal human progenitor cells and in
499 acute myeloid leukaemia. Leukemia 2007;**21**:2495-505.

500 (12) Omidvar N, Kogan S, Beurlet S, le PC, Janin A, West R, et al. BCL-2 and mutant NRAS
501 interact physically and functionally in a mouse model of progressive myelodysplasia.
502 Cancer Res 2007;**67**:11657-67.

503 (13) Gao J, Aksoy BA, Dogrusoz U, Dresdner G, Gross B, Sumer SO, et al. Integrative
504 analysis of complex cancer genomics and clinical profiles using the cBioPortal. Sci
505 Signal 2013;**6**:l1.

506 (14) Cerami E, Gao J, Dogrusoz U, Gross BE, Sumer SO, Aksoy BA, et al. The cBio cancer
507 genomics portal: an open platform for exploring multidimensional cancer genomics data.
508 Cancer Discov 2012;**2**:401-4.

509 (15) Ley TJ, Miller C, Ding L, Raphael BJ, Mungall AJ, Robertson A, et al. Genomic and
510 epigenomic landscapes of adult de novo acute myeloid leukemia. N Engl J Med
511 2013;**368**:2059-74.

512 (16) Mikawa T, LLeonart ME, Takaori-Kondo A, Inagaki N, Yokode M, Kondoh H.
513 Dysregulated glycolysis as an oncogenic event. Cell Mol Life Sci 2015;**72**:1881-92.

514 (17) Altenhofer S, Kleikers PW, Radermacher KA, Scheurer P, Rob Hermans JJ, Schiffers P,
515 et al. The NOX toolbox: validating the role of NADPH oxidases in physiology and
516 disease. Cell Mol Life Sci 2012;**69**:2327-43.

517 (18) Beckman JS, Minor RL, Jr., White CW, Repine JE, Rosen GM, Freeman BA. Superoxide
518 dismutase and catalase conjugated to polyethylene glycol increases endothelial enzyme
519 activity and oxidant resistance. J Biol Chem 1988;**263**:6884-92.

520 (19) Ros S, Schulze A. Balancing glycolytic flux: the role of 6-phosphofructo-2-
521 kinase/fructose 2,6-bisphosphatases in cancer metabolism. Cancer Metab 2013;**1**:8.

522 (20) Yalcin A, Clem BF, Simmons A, Lane A, Nelson K, Clem AL, et al. Nuclear targeting of
523 6-phosphofructo-2-kinase (PFKFB3) increases proliferation via cyclin-dependent
524 kinases. J Biol Chem 2009;**284**:24223-32.

525 (21) Echtay KS, Roussel D, St-Pierre J, Jekabsons MB, Cadenas S, Stuart JA, et al.
526 Superoxide activates mitochondrial uncoupling proteins. Nature 2002;**415**:96-9.

527 (22) Domenech E, Maestre C, Esteban-Martinez L, Partida D, Pascual R, Fernandez-Miranda
528 G, et al. AMPK and PFKFB3 mediate glycolysis and survival in response to mitophagy
529 during mitotic arrest. Nat Cell Biol 2015;**17**:1304-16.

530 (23) Mailloux RJ, Adjeitey CN, Harper ME. Genipin-induced inhibition of uncoupling
531 protein-2 sensitizes drug-resistant cancer cells to cytotoxic agents. PLoS One
532 2010;**5**:e13289.

533 (24) Clem B, Telang S, Clem A, Yalcin A, Meier J, Simmons A, et al. Small-molecule
534 inhibition of 6-phosphofructo-2-kinase activity suppresses glycolytic flux and tumor
535 growth. Mol Cancer Ther 2008;**7**:110-20.

536 (25) Clem BF, O'Neal J, Tapolsky G, Clem AL, Imbert-Fernandez Y, Kerr DA, et al.
537 Targeting 6-phosphofructo-2-kinase (PFKFB3) as a therapeutic strategy against cancer.
538 Mol Cancer Ther 2013;**12**:1461-70.

539 (26) Stanicka J, Russell EG, Woolley JF, Cotter TG. NADPH oxidase-generated hydrogen
540 peroxide induces DNA damage in mutant FLT3-expressing leukemia cells. J Biol Chem
541 2015;**290**:9348-61.

542 (27) Tang CT, Lin XL, Wu S, Liang Q, Yang L, Gao YJ, et al. NOX4-driven ROS formation
543 regulates proliferation and apoptosis of gastric cancer cells through the GLI1 pathway.
544 Cell Signal 2018;**46**:52-63.

545 (28) Paik JY, Jung KH, Lee JH, Park JW, Lee KH. Reactive oxygen species-driven HIF1alpha
546 triggers accelerated glycolysis in endothelial cells exposed to low oxygen tension. Nucl
547 Med Biol 2017;**45**:8-14.

548 (29) Koppenol WH, Bounds PL, Dang CV. Otto Warburg's contributions to current concepts
549 of cancer metabolism. Nat Rev Cancer 2011;**11**:325-37.

550 (30) Prata C, Maraldi T, Fiorentini D, Zambonin L, Hakim G, Landi L. Nox-generated ROS
551 modulate glucose uptake in a leukaemic cell line. Free Radic Res 2008;**42**:405-14.

552 (31) Macheda ML, Rogers S, Best JD. Molecular and cellular regulation of glucose
553 transporter (GLUT) proteins in cancer. J Cell Physiol 2005;**202**:654-62.

554 (32) Chen WL, Wang JH, Zhao AH, Xu X, Wang YH, Chen TL, et al. A distinct glucose
555 metabolism signature of acute myeloid leukemia with prognostic value. Blood
556 2014;**124**:1645-54.

557 (33) Wang Y, Zhang L, Chen WL, Wang JH, Li N, Li JM, et al. Rapid diagnosis and
558 prognosis of de novo acute myeloid leukemia by serum metabonomic analysis. J
559 Proteome Res 2013;**12**:4393-401.

560 (34) Adane B, Ye H, Khan N, Pei S, Minhajuddin M, Stevens BM, et al. The Hematopoietic
561 Oxidase NOX2 Regulates Self-Renewal of Leukemic Stem Cells. Cell Rep 2019;**27**:238-
562 54.

563 (35) Shanmugam M, McBrayer SK, Rosen ST. Targeting the Warburg effect in hematological
564 malignancies: from PET to therapy. Curr Opin Oncol 2009;**21**:531-6.

565 (36) Atsumi T, Chesney J, Metz C, Leng L, Donnelly S, Makita Z, et al. High expression of
566 inducible 6-phosphofructo-2-kinase/fructose-2,6-bisphosphatase (iPFK-2; PFKFB3) in
567 human cancers. Cancer Res 2002;**62**:5881-7.

568 (37) Li HM, Yang JG, Liu ZJ, Wang WM, Yu ZL, Ren JG, et al. Blockage of glycolysis by
569 targeting PFKFB3 suppresses tumor growth and metastasis in head and neck squamous
570 cell carcinoma. J Exp Clin Cancer Res 2017;**36**:7.

571 (38) Kim SG, Manes NP, El-Maghrabi MR, Lee YH. Crystal structure of the hypoxia-
572 inducible form of 6-phosphofructo-2-kinase/fructose-2,6-bisphosphatase (PFKFB3): a
573 possible new target for cancer therapy. J Biol Chem 2006;**281**:2939-44.

574 (39) Marsin AS, Bouzin C, Bertrand L, Hue L. The stimulation of glycolysis by hypoxia in
575 activated monocytes is mediated by AMP-activated protein kinase and inducible 6-
576 phosphofructo-2-kinase. J Biol Chem 2002;**277**:30778-83.

577 (40) Haddad JJ, Land SC. A non-hypoxic, ROS-sensitive pathway mediates TNF-alpha-
578 dependent regulation of HIF-1alpha. FEBS Lett 2001;**505**:269-74.

579 (41) Chesney J, Telang S. Regulation of glycolytic and mitochondrial metabolism by ras. Curr
580 Pharm Biotechnol 2013;**14**:251-60.

581 (42) Yalcin A, Telang S, Clem B, Chesney J. Regulation of glucose metabolism by 6-
582 phosphofructo-2-kinase/fructose-2,6-bisphosphatases in cancer. Exp Mol Pathol
583 2009;**86**:174-9.

584 (43) Shi SY, Lu SY, Sivasubramaniyam T, Revelo XS, Cai EP, Luk CT, et al. DJ-1 links
585 muscle ROS production with metabolic reprogramming and systemic energy homeostasis
586 in mice. Nat Commun 2015;**6**:7415.

587 (44) Novellasdemunt L, Bultot L, Manzano A, Ventura F, Rosa JL, Vertommen D, et al.
588 PFKFB3 activation in cancer cells by the p38/MK2 pathway in response to stress stimuli.
589 Biochem J 2013;**452**:531-43.

590 (45) Thompson MP, Kim D. Links between fatty acids and expression of UCP2 and UCP3
591 mRNAs. FEBS Lett 2004;**568**:4-9.

592 (46) Carracedo A, Cantley LC, Pandolfi PP. Cancer metabolism: fatty acid oxidation in the
593 limelight. Nat Rev Cancer 2013;**13**:227-32.

594 (47) Liu X, Zheng H, Yu WM, Cooper TM, Bunting KD, Qu CK. Maintenance of mouse
595 hematopoietic stem cells ex vivo by reprogramming cellular metabolism. Blood
596 2015;**125**:1562-5.

597 (48) Ito K, Carracedo A, Weiss D, Arai F, Ala U, Avigan DE, et al. A PML-PPAR-delta
598 pathway for fatty acid oxidation regulates hematopoietic stem cell maintenance. Nat Med
599 2012;**18**:1350-8.

600 (49) Lu L, Chen Y, Zhu Y. The molecular basis of targeting PFKFB3 as a therapeutic strategy
601 against cancer. Oncotarget 2017;**8**:62793-802.

602 (50) Zhu W, Ye L, Zhang J, Yu P, Wang H, Ye Z, et al. PFK15, a Small Molecule Inhibitor of
603 PFKFB3, Induces Cell Cycle Arrest, Apoptosis and Inhibits Invasion in Gastric Cancer.
604 PLoS One 2016;**11**:e0163768.

605 (51) O'Neal J, Clem A, Reynolds L, Dougherty S, Imbert-Fernandez Y, Telang S, et al.
606 Inhibition of 6-phosphofructo-2-kinase (PFKFB3) suppresses glucose metabolism and the
607 growth of HER2+ breast cancer. Breast Cancer Res Treat 2016;**160**:29-40.

608 (52) Reddy MM, Fernandes MS, Deshpande A, Weisberg E, Inguilizian HV, Abdel-Wahab O,
609 et al. The JAK2V617F oncogene requires expression of inducible
610 phosphofructokinase/fructose-bisphosphatase 3 for cell growth and increased metabolic
611 activity. Leukemia 2012;**26**:481-9.

612

613 ## Figure Legends

614 **Figure 1. NOX-derived ROS promotes transcriptional change in N-RAS^{G12D} expressing**
615 **HSPC and AML patient blasts and identifies the glycolytic pathway as a major target of**
616 **ROS. (A)** Summary flow diagram showing the strategy for changes in mRNA expression
617 analysed by Affymetrix microarray. Four treatment conditions were employed for the
618 examination of the effect of N-RAS^{G12D} and ROS on mRNA gene expression: CD34^{+} HSPC
619 infected with control vector ('C') or N-RAS^{G12D} ('N'), incubated in the presence or absence of
620 100nM DPI for 24 h to determine the ROS-specific gene expression profile (n=4). We examined
621 changes that were only co-directional (i.e. they were similarly dysregulated in each replicate).
622 **(B)** Significantly changing GeneGo^{TM} Maps in human HSPCs as a response to changes in
623 exposure to ROS. **(C)** Statistically significant changes in mRNA showing the impact of DPI
624 (unfilled bars) on N-RAS^{G12D} dependent target gene expression (filled bars). Non-specific
625 effects of DPI were excluded as described in (A). Only genes involved in carbohydrate
626 metabolism using the Human Exon 1.0ST Full Probe Set list were analysed. Statistically
627 significant gene changes in Control cells treated with DPI compared to untreated control were
628 excluded from the final list. Data represents mean fold change of n=4; P value calculated by 2-
629 way ANOVA with Bonferroni multiple testing correction. **(D)** Hierarchical clustering of patient
630 AML mRNA expression z-Scores based on RNA Seq V2 RSEM. NOX2 high / low expressing
631 blasts was defined as, above and below the median expression intensity of NOX2 (aka *CYBB*).
632 Genes involved in glycolysis and carbohydrate transport are shown (as defined by Affymetrix
633 Netaffx^{TM} gene annotation software under advanced pathway searches); AML patient blasts

634 (n=160). Boxed section shows cluster of genes associated with NOX2 high AML blasts. **(E)**
635 Expression of genes from AML patient blasts significantly correlating with NOX2 (*CYBB,*
636 R>0.5) expression. R; Spearmans Correlation co-efficient. FDR, False Discovery Rate; GLUT3
637 (SLC2A3), glucose transporter 3; GLUT5 (SLC2A5), glucose transporter 5; GLUT6 (SLC2A6),
638 glucose transporter 6; GLUT14 (SLC2A14), glucose transporter 14; HK, hexokinase; PFKFB, 6-
639 phosphofructo-2-kinase/fructose-2,6-biphosphatase; PFK(P). phosphofructokinase platelet;
640 FBP1, fructose-1,6-bisphosphatase 1; ENO, enolase; PK(M), pyruvate kinase muscle; LDH(A),
641 lactate dehydrogenase A; MCT4 (SLC16A3), monocarboxylate transporter 4.

642 **Figure 2. ROS promotes glucose uptake. (A)** 'Medium' - following transduction, N-RAS^{G12D}
643 were cultured for 3 days without growth factors, glucose present in the media was assayed using
644 a fluorometric glucose kit (n=4) (see methods) and normalised to empty-vector control. Glucose
645 uptake in the cell is inversely proportional to the glucose remaining in the media. '2-NBDG' -
646 glucose uptake using the fluorogenic substrate 2-NBDG (normalised to control) in N-RAS^{G12D}
647 HSPC (n=4) cultured as above. **(B)** Glucose uptake (normalised to Wild Type (WT) control) *ex*
648 *vivo* in N-RAS^{G12D} bone marrow compared to WT control cells (n=8). **(C)** N-RAS^{G12D} HSPCs
649 (day 5 post infection) were treated with 100nm DPI and cultured for 24 h without growth factors.
650 Glucose in culture media (normalised to untreated control) was assayed (n=3). Glucose uptake
651 in the cell is inversely proportional to the glucose remaining in the media. N-RAS^{G12D} HSPCs
652 were treated with 5μM VAS-2870 (VAS; n=3) or 300mU/mL PEGylated catalase (Cat; n=2) for
653 24 h and glucose uptake assayed using 2-NBDG (normalised to PEG-treated control). **(D)**
654 Concentration of extracellular L-lactate in culture media of transduced CD34^{+} cells (cultured as

655 above) treated with 5 μM VAS-2870 as above (n=4). Data represents mean±1SD. * denotes
656 $p<0.05$ and ** $p<0.001$ analysed by one sample t-test.

657 **Figure 3. Overproduction of ROS is associated with changes in glucose utilizations in**
658 **primary AML blasts.** Data from global biochemical profiling of AML blasts stratified
659 according to extracellular ROS production was performed. **(A)** Principal components analysis of
660 global biochemical profiling of AML cells with high and low ROS production; ROS^{Low}, n=10;
661 ROS^{high}, n=10. Also shown are normal human mononuclear control cells (Ctrl_MN: n=4). **(B)**
662 Summary of the numbers of biochemicals that achieved statistical significance (*$p\leq0.05$), as well
663 as those approaching significance ($^{\#\#}0.05<p<0.10$) analysed by Welch's two sample t-test.
664 Levels of biochemicals normalised to total protein in **(C)** glycolysis and **(D)** Pentose Phosphate
665 Pathway (PPP) are shown.

666 **Figure 4. PFKFB3 protein expression correlates with levels of NOX2 derived extracellular**
667 **ROS.** **(A)** Human $CD34^+$ HSPC control and N-RAS^{G12D} (day 5 post transduction) were cultured
668 for 24 h in cytokine free media in the presence or absence of DPI (100nM) followed by whole
669 cell protein extraction. (i) Example western blot of PFKFB3 protein expression. (ii) Relative
670 protein expression (as measured by pixel densitometry of equivalent regions of interest (ROI)
671 between different samples on the same blot then normalised to control) of PFKFB3 (n=3). **(B)**
672 Western blot showing PFKFB3 protein expression levels in THP-1 cells with NOX2 knocked
673 down (KD) or cells treated with DPI (100nM) for 24 h compared to control (non-mammalian
674 shRNA) cells. Lower panel showing relative protein expression of PFKFB3 compared to control
675 (n=3). **(C)** Percentage proliferative change (normalised to control) in THP-1 cells with NOX2
676 KD (n>3) over 72 h. **(D)** Glucose uptake in single cell analysis using 2-NBDG (normalised to

677 control) in THP-1 cells with NOX2 KD (n=4) or THP-1 cells treated with 300 mU/mL
678 PEGylated catalase (Cat; n=6). **(E)** Western blot showing PFKFB3 protein expression in
679 Mv4;11 cells treated with glucose oxidase (GOX) (10 and 20mU/mL for 24 h), which catalyses
680 production of hydrogen peroxide (H_2O_2) in cell culture media; (imitating the effect of NOX2-
681 generated ROS production). Lower panel showing relative protein expression of PFKFB3
682 compared to control (n=3). Correlation of PFKFB3 overexpression in Mv4;11 cells treated with
683 GOX for 24 h on **(F)** proliferation and **(G)** glucose uptake using 2-NDBG (n=5). Actin was used
684 as a loading control. Data represents mean±1SD. † denotes $p<0.05$ analysed by ANOVA with
685 Tukey's honestly significance difference. * denotes $p<0.05$ analysed by one sample t-test.

686 **Figure 5. Effect of PFKFB3 overexpression and knock down on proliferation and glucose**
687 **uptake in leukemia cells. (A)** Western blot analysis of PFKFB3 protein comparing control and
688 PFKFB3-overexpression (OE) Mv4;11 cells. Actin was used as a loading control. **(B)**
689 Percentage proliferation (normalised to control) of Mv4;11 PFKFB3 over-expressed (OE) cells
690 compared to control (n>3). **(C)** Glucose uptake in Mv4;11 PFKFB3-OE cells compared to
691 control following 72 h (n=3). Glucose was assayed in the culture media and glucose uptake in
692 the cell is inversely proportional to the glucose remaining in the media. The concentration of
693 glucose in the culture media (starting concentration 25nmol/μL) of PFKFB3-OE cells after 24 h
694 was 15nmol/μL compared with 23nmol/μL in control cells. **(D)** Western blot analysis of
695 PFKFB3 protein comparing control (non-mammalian targeting shRNA control) and PFKFB3
696 knock down (KD) in THP-1 cells. Actin was used as a loading control. **(E)** Percentage
697 proliferation (normalised to control) of THP-1 PFKFB3-KD cells compared to control (n>3). **(F)**
698 Glucose uptake in single cell analysis using 2-NBDG (normalised to control) of THP-1
699 PFKFB3-KD cells compared to control following 24h growth (n=5). Data represents

700 mean±1SD. † denotes $p<0.05$ analysed by ANOVA with Tukey's honestly significance

701 difference. $^{***}p<0.005$ denotes statistical significance calculated by Student's t-test calculated.

702 **Figure 6. ROS induced changes in PFKFB3 expression is mediated via UCP/p-AMPK. (A)**

703 Normalised $\log_2$ expression of *HIFA* (transcript ID 3567728) mRNA in control HSPC, DPI, N-

704 RAS^{G12D} HSPC and N-RAS^{G12D} HSPC treated with DPI (100nM). Box plots represent median

705 quartile ranges, x represents mean value (n=4). p-Value calculated by 2-way ANOVA with

706 Bonferroni multiple testing correction. **(B)**(i) Western blot showing expression of HIF-1α in

707 control THP-1, THP-1 NOX2-KD and THP-1 cells treated with DPI as (A). As positive

708 controls, THP-1 cells were treated with $CoCl_2$ as indicated (an inhibitor of HIF-1α degradation

709 (50)). HIF-1α recombinant protein were also immunoblotted. Actin was used as loading control**.**

710 **(B)**(ii) Western blot showing expression of HIF-1α, comparing control THP-1 (non-mammalian

711 shRNA target) and THP-1 HIF-1α knocked down (KD). Cells were also untreated or treated

712 with $CoCl_2$ as above. **(C)** Western blot showing expression of PFKFB3 in THP-1 cells knocked

713 down with HIF1-α. **(D)** Glucose uptake (normalised to control) of THP HIF-1α KD cells (n=3).

714 Data represents mean±1SD. **(E)** Immunoblot showing PFKFB3, UCP2 and p-AMPK expression

715 upon 1 h pre-treatment of Mv4;11 cells with the UCP2 inhibitor Genipin (5μM) followed by

716 GOX treatment for 24 h. **(F)** Glucose uptake using 2-NBDG (normalised to untreated cells;

717 control) of Mv4;11 cells treated with GOX (20mU/mL) and / or Genipin (5μM) (n=5). Data

718 represents mean±1SD. $^{***}p<0.005$ and $^{§}p<0.01$ denotes statistical significance calculated by

719 Student's t-test calculated.

720 **Figure 7. Targeting PFKFB3 reduces glucose uptake and cell proliferation in AML cells.**

721 Glucose uptake using 2NBDG (normalised to untreated control) in THP-1 cells lines treated with

722 **(A)** 3PO or **(B)** PFK158 for 24 h. Vehicle control for 3PO and PFK158 was DMSO 0.05% and
723 DMSO 0.01% respectively. Data represents mean±1SD (n>3). Proliferation (normalised to
724 control) in THP-1 cells, seeded at 4 x 10^5/mL treated with **(C)** 3PO or **(D)** PFK158. Vehicle
725 control for 3PO, DMSO 0.05% (n=6). Vehicle control for PFK158, DMSO 0.01% (n=6). **(E)**
726 Glucose uptake using 2NBDG (normalised to untreated control) in Mv4;11 cells treated with
727 inhibitors to PFKFB3 and/or incubated with 10 mU/mL GOX (source of H_2O_2) (n=3). **(F)**
728 Representative flow cytometric bivariate plots from bone marrow harvested from tibias and
729 femurs of adult NSG mice (7-10 weeks old) sub-lethally irradiated with 200cGy total body
730 irradiation 24 h before injection of control THP-1 cells or THP-1 cells where PFKFB3 was KD.
731 Human cells were distinguished from mouse cells using hCD45-FITC, hCD33-APC and
732 mCD45-PerCP-Cy5.5 antibodies. Uninoculated NSG mice were used to control for the analysis
733 of THP-1 engraftment (n=4) and analysed at week 6. Data represents mean±1SD. † denotes
734 $p<0.05$ and represent significantly different groups from control, analysed by ANOVA with
735 Tukey's honestly significance difference. $^{***}p<0.005$ denotes statistical significance calculated
736 by Student's t-test calculated.

A

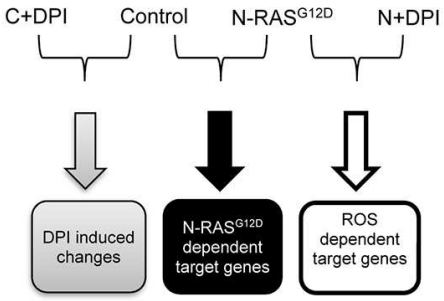

B

#	GeneGo^{TM} Pathway Maps	p-value	FDR
1	Glycolysis and gluconeogenesis (short map)	1.982e-8	8.324e-7
2	Fructose metabolism	2.448e-6	5.141e-5
3	Fructose metabolism/ Rodent version	4.101e-6	5.741e-5
4	Glycolysis and gluconeogenesis p. 1	3.208e-5	3.368e-4
5	Development regulation of endothelial progenitor cell differentiation from adult stem cells	3.000e-3	2.520e-2
6	Urea cycle	4.197e-3	2.882e-2
7	(L)-Arginine metabolism	4.804e-3	2.882e-2
8	Arginine metabolism/ Rodent version	6.999e-3	3.675e-2
9	Glycine, serine, cysteine and threonine metabolism	1.212e-2	5.251e-2
10	Glycine, serine, cysteine and threonine metabolism/ Rodent version	1.250e-2	5.251e-2

C

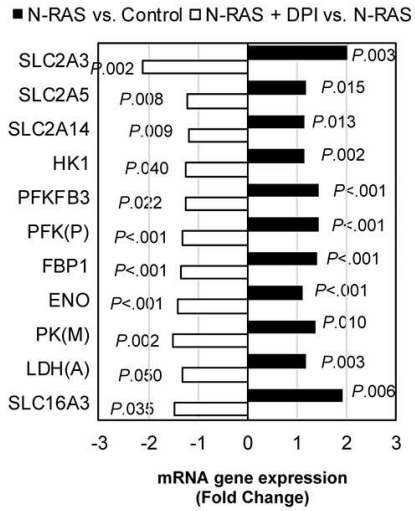

D

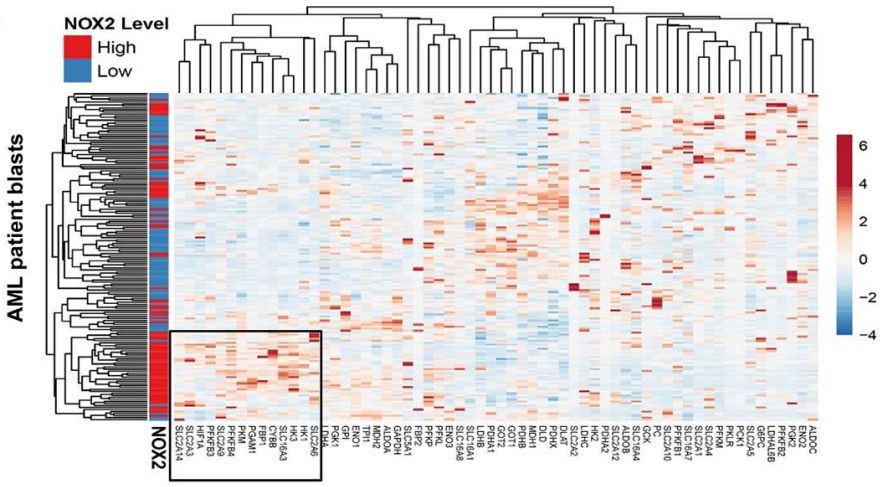

E

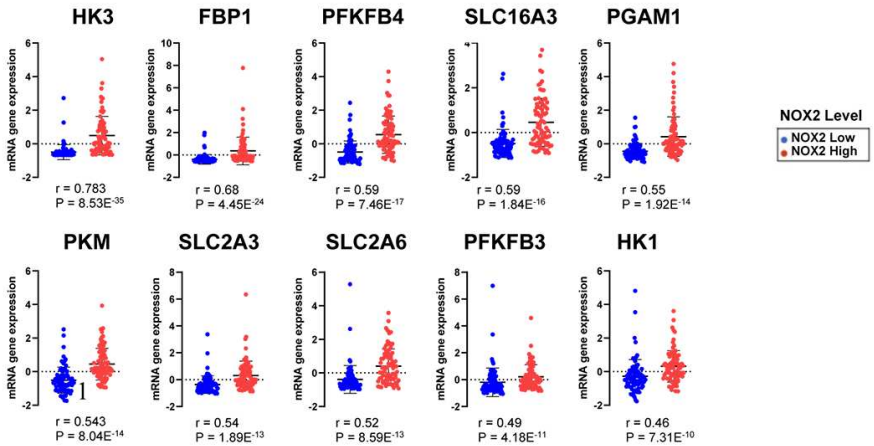

Figure 1

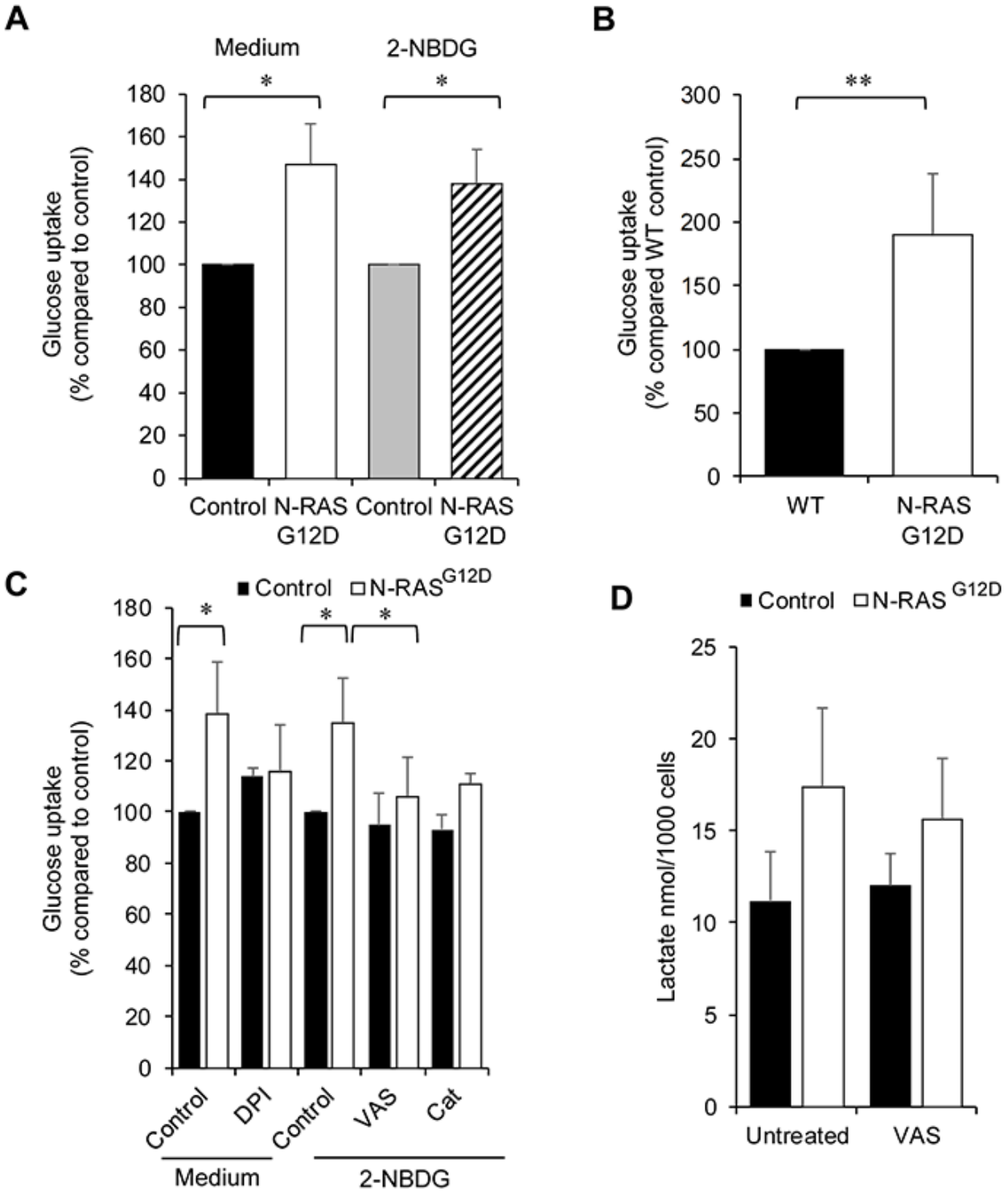
A
Medium
2-NBDG
Glucose uptake
(% compared to control)
Control
N-RAS G12D
Control
N-RAS G12D
B
Glucose uptake
(% compared WT control)
WT
N-RAS G12D
C
Control
N-RAS G12D
Glucose uptake
(% compared to control)
Control
DPI
Control
VAS
Cat
Medium
2-NBDG
D
Control
N-RAS G12D
Lactate nmol/1000 cells
Untreated
VAS

Figure 2.

A

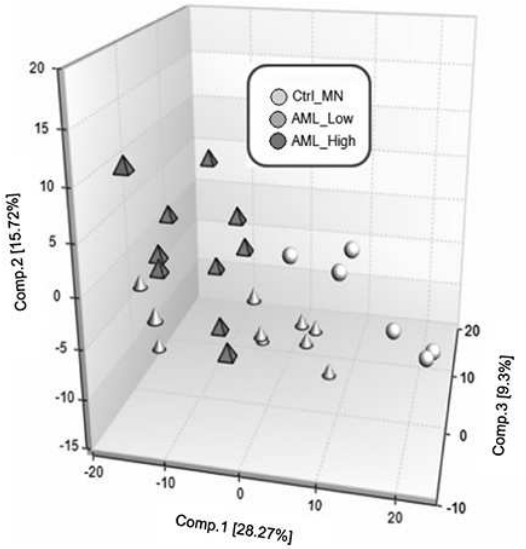

B

Significantly altered Biochemicals	Total Biochemicals P≤0.05	Biochemicals (↑/↓)	Total Biochemicals 0.05<p<0.10	Biochemicals (↑/↓)
AML ROS^{Low} / Ctrl MN	208	172/36	101	76/25
AML ROS^{High} / Ctrl MN	268	240/28	94	76/18
AML ROS^{High} / AML ROS^{Low}	97	76/21	99	66/33

C

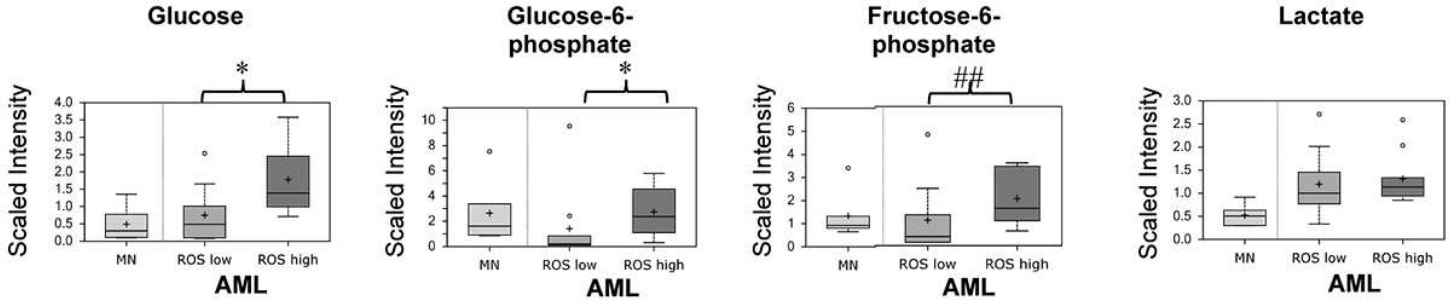

D

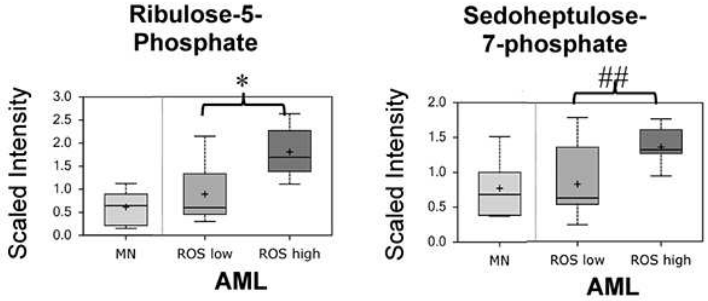

Figure 3.

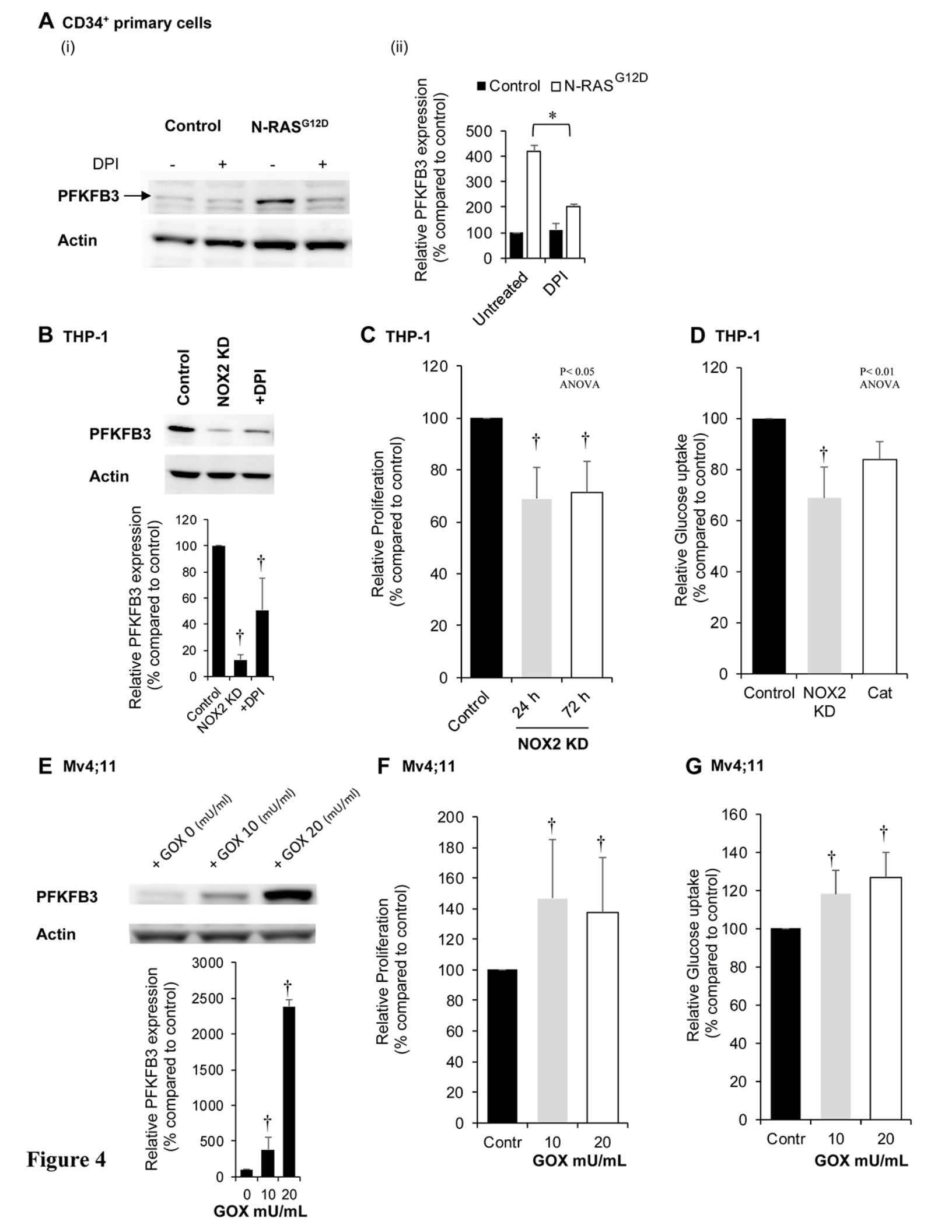
A CD34+ primary cells
(i)
Control
N-RAS G12D
DPI
-
+
-
+
PFKFB3
Actin
(ii)
Control
N-RAS G12D
Relative PFKFB3 expression (% compared to control)
*
Untreated
DPI
B THP-1
Control
NOX2 KD
+DPI
PFKFB3
Actin
Relative PFKFB3 expression (% compared to control)
C THP-1
P< 0.05 ANOVA
Relative Proliferation (% compared to control)
Control
24 h
72 h
NOX2 KD
D THP-1
P< 0.01 ANOVA
Relative Glucose uptake (% compared to control)
Control
NOX2 KD
Cat
E Mv4;11
+ GOX 0 (mU/ml)
+ GOX 10 (mU/ml)
+ GOX 20 (mU/ml)
PFKFB3
Actin
Relative PFKFB3 expression (% compared to control)
GOX mU/mL
F Mv4;11
Relative Proliferation (% compared to control)
Contr
10
20
GOX mU/mL
G Mv4;11
Relative Glucose uptake (% compared to control)
Contr
10
20
GOX mU/mL

Figure 4

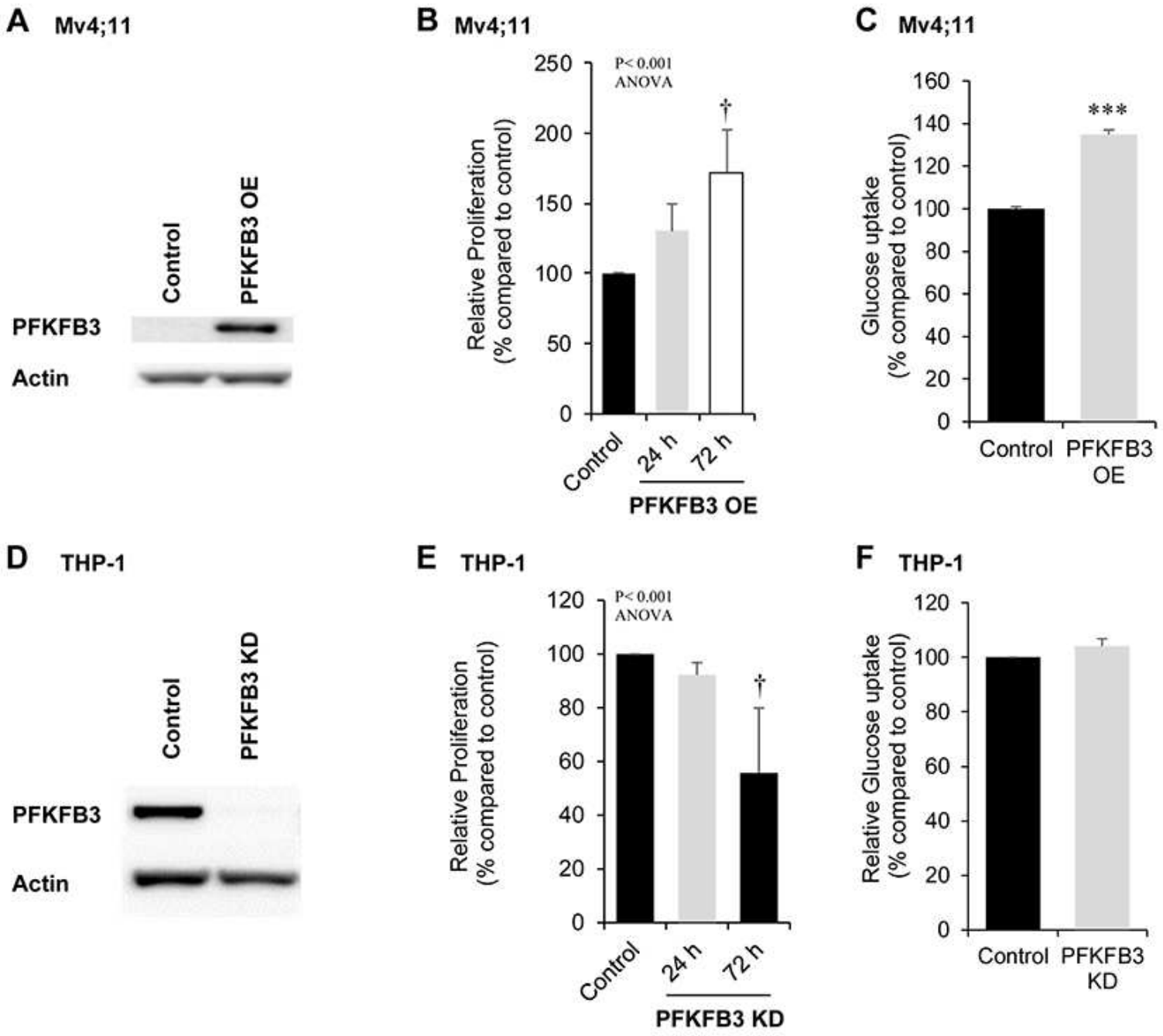
A Mv4;11
Control
PFKFB3 OE
PFKFB3
Actin
B Mv4;11
P< 0.001
ANOVA
Relative Proliferation
(% compared to control)
250
200
150
100
50
0
†
Control
24 h
72 h
PFKFB3 OE
C Mv4;11
Glucose uptake
(% compared to control)
160
140
120
100
80
60
40
20
0
***
Control
PFKFB3
OE
D THP-1
Control
PFKFB3 KD
PFKFB3
Actin
E THP-1
P< 0.001
ANOVA
Relative Proliferation
(% compared to control)
120
100
80
60
40
20
0
†
Control
24 h
72 h
PFKFB3 KD
F THP-1
Relative Glucose uptake
(% compared to control)
120
100
80
60
40
20
0
Control
PFKFB3
KD

Figure 5.

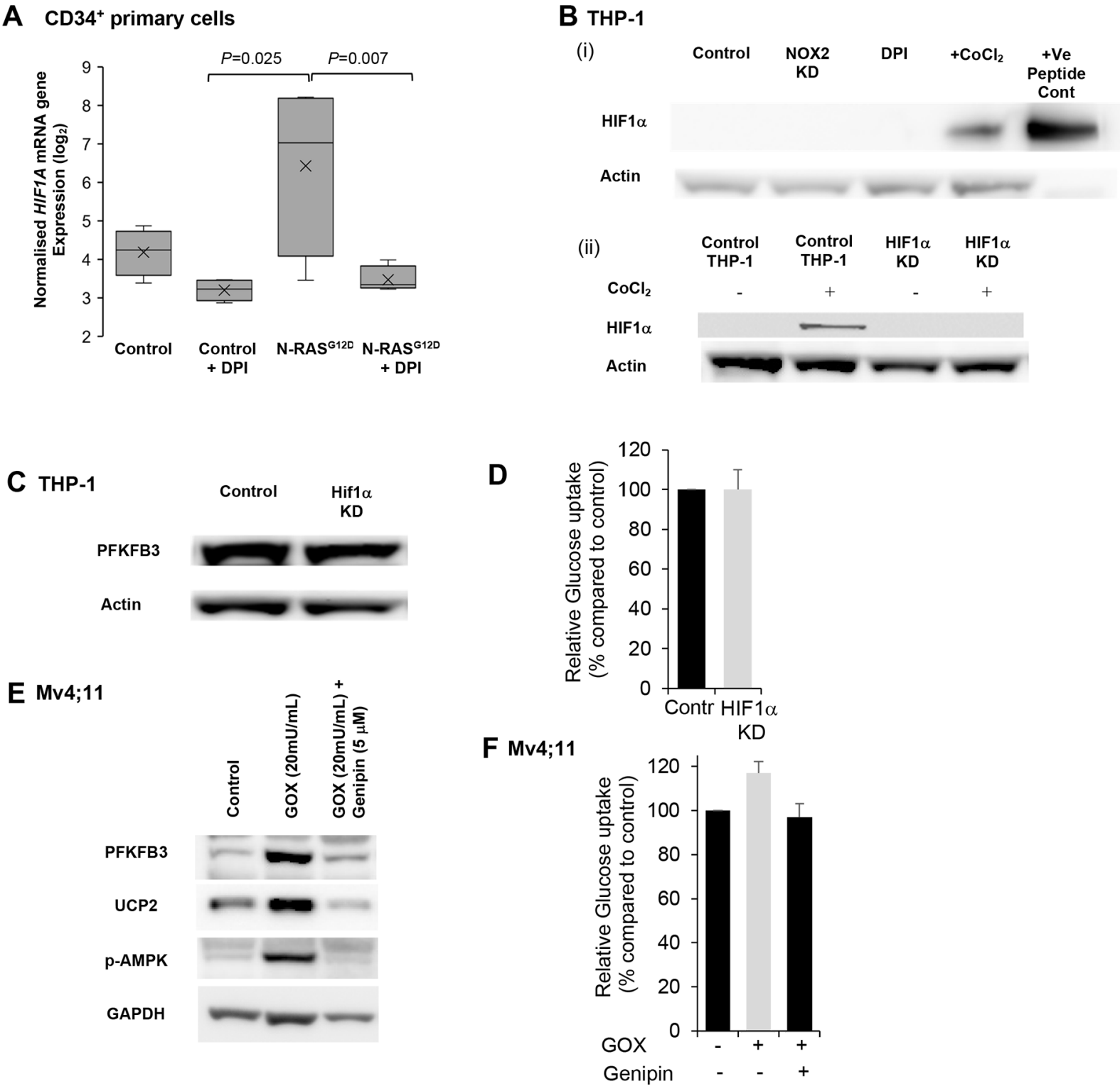
A CD34+ primary cells
P=0.025
P=0.007
Normalised HIF1A mRNA gene Expression (log2)
9
8
7
6
5
4
3
2
Control
Control + DPI
N-RASG12D
N-RASG12D + DPI
B THP-1
(i)
Control
NOX2 KD
DPI
+CoCl2
+Ve Peptide Cont
HIF1α
Actin
(ii)
Control THP-1
Control THP-1
HIF1α KD
HIF1α KD
CoCl2
-
+
-
+
HIF1α
Actin
C THP-1
Control
Hif1α KD
PFKFB3
Actin
D
Relative Glucose uptake (% compared to control)
120
100
80
60
40
20
0
Contr
HIF1α KD
E Mv4;11
Control
GOX (20mU/mL)
GOX (20mU/mL) + Genipin (5 μM)
PFKFB3
UCP2
p-AMPK
GAPDH
F Mv4;11
Relative Glucose uptake (% compared to control)
120
100
80
60
40
20
0
GOX
-
+
+
Genipin
-
-
+

Figure 6.

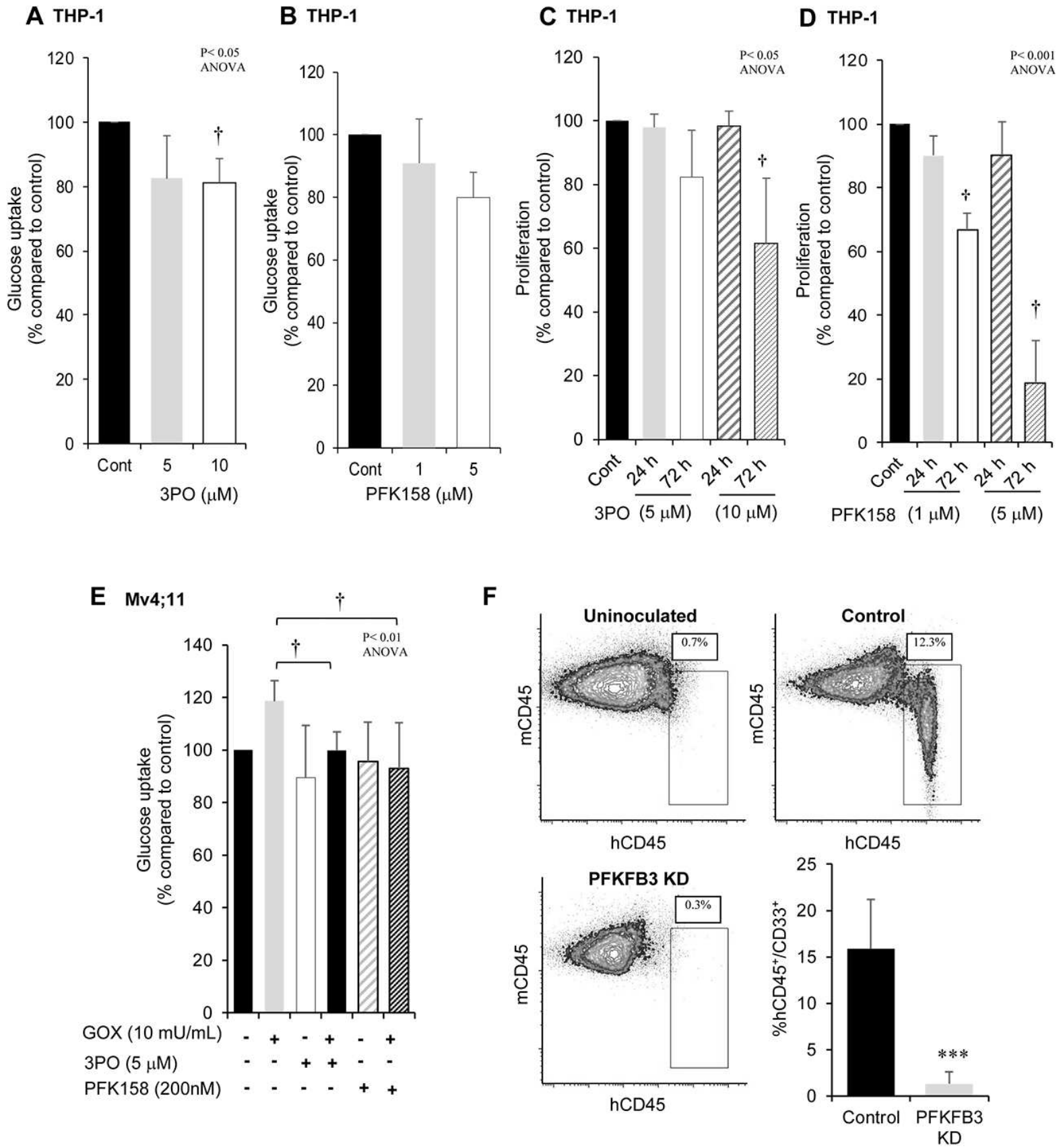
A THP-1
P< 0.05
ANOVA
Glucose uptake
(% compared to control)
Cont
5
10
3PO (μM)
B THP-1
Glucose uptake
(% compared to control)
Cont
1
5
PFK158 (μM)
C THP-1
P< 0.05
ANOVA
Proliferation
(% compared to control)
Cont
24 h
72 h
24 h
72 h
3PO (5 μM)
(10 μM)
D THP-1
P< 0.001
ANOVA
Proliferation
(% compared to control)
Cont
24 h
72 h
24 h
72 h
PFK158 (1 μM)
(5 μM)
E Mv4;11
P< 0.01
ANOVA
Glucose uptake
(% compared to control)
GOX (10 mU/mL)
3PO (5 μM)
PFK158 (200nM)
F
Uninoculated
0.7%
Control
12.3%
PFKFB3 KD
0.3%
mCD45
hCD45
%hCD45+/CD33+
***
Control
PFKFB3
KD

Figure 7